American Mineralogist, Volume 76, pages 1389–1399, 1991

The kentrolite-melanotekite series, $4Pb_2(Mn,Fe)_2^{3+}O_2[Si_2O_7]$: Chemical crystallographic relations, lone-pair splitting, and cation relation to $8URe_2$

Paul Brian Moore
Department of the Geophysical Sciences, The University of Chicago, Chicago, Illinois 60637, U.S.A.
Pradip K. Sen Gupta
Department of Geology, Memphis State University, Memphis, Tennessee 38152, U.S.A.
Jinchuan Shen
China University of Geosciences, Wuhan 430074, Peoples Republic of China
Elmer O. Schlemper
Department of Chemistry, University of Missouri, Columbia, Missouri 65211, U.S.A.

Abstract

Members of the kentrolite-melanotekite series from Långban, Sweden, are orthorhombic holosymmetric, $a = 6.961(2)$, $b = 11.018(3)$, $c = 9.964(5)$ Å, space group *Pbcn* (subgroup of *Cmcm*), $Z = 4$, formula from Cameca probe analysis and refined structure $Pb_2(Mn_{0.68}Fe_{0.32})_2^{3+}O_2[Si_2O_7]$. The structure has been refined to $R = 0.047$ for 1031 reflections.

The $[(Mn,Fe)_2^{3+}O_2Si_2O_7]$ fraction, the simple part, is based on $^1_\infty[M^{3+}O_4]$ edge-sharing octahedral chains parallel to [001]. These octahedra are alternately *cis* and *trans* with respect to adjacent octahedra, reminiscent of the structure of synthetic CMS-X1, $Ca_3Mn_2^{3+}O_2[Si_4O_{12}]$. The oligosilicate dimers Si-O-Si are aligned nearly parallel to [100]. Their role is reminiscent of similar units in structures included in Belov's second chapter on silicates.

The $6s^2$ Pb^{2+} lone-pair cations are split in an unexpected fashion, and this splitting was the source of the problems in structure solution. $R \sim 0.14$ typifies one Pb centroid alone. Gradual refinement of data from a ground sphere converged to 0.73 Pb(1) and 0.27 Pb(2), populated in a complementary fashion, with Pb(1) − Pb(2) separation of 0.56 Å. Noteworthy is the unsymmetrical splitting of the Pb atoms.

Bond distance averages are $^{[6]}M(1)^{3+}$-O = 2.01 (prolate spheroid), $^{[6]}M(2)^{3+}$-O = 2.03 (oblate spheroid), $^{[4]}$Si-O = 1.63, $^{[6]}$Pb(1)-O = 2.40–2.99, ⟨2.60⟩, and $^{[6]}$Pb(2)-O = 2.27–3.02, ⟨2.63⟩ Å. Five cations and five anions comprise the asymmetric unit. Dominant $4d^4$ Mn^{3+} at M(1) and M(2) evince tetragonal Jahn-Teller distortion of the coordination polyhedra as elongated (prolate) and compressed (oblate) octahedra, respectively.

The kentrolite-melanotekite structure type is another where cations show a close relationship to an intermetallic phase, in this case low URe_2. For Pb(1), Pb(2), M(1), M(2), and Si cations and U, U, Re(1), Re(2), and Re(3) atoms, the mean difference between atom coordinates, scaled to the kentrolite cell, is $\Delta = 0.27$ Å with range 0.00–0.48 Å.

Introduction

The history of studies of the kentrolite-melanotekite series is long and problematical. This is somewhat surprising as they have relatively simple compositions, but their chemical crystallographic relations are still undescribed. Kentrolite, from the Greek *kentron* = thorn, was originally described and named by Damour and vom Rath (1881). They culled thornlike crystals from a suite of specimens collected earlier at some unspecified locality in southern Chile. They proposed either $Pb_2^{2+}Mn_2^{3+}Si_2O_9$ or $Pb^{2+}Mn^{4+}SiO_5$ as possible formulas. Lindström (1880) christened a new black silicate from Långban, Sweden, as melanotekite, from the Greek *melanos* + *tektos* = black glass, and he demonstrated that it was the Fe analogue of kentrolite. Flink (1891) reported kentrolite from Långban, thus completing the cycle, with the two end-members of a relatively simple series occurring at one locality. Since then, diverse occurrences have been reported; the occurrence at Hillsboro, New Mexico (Warren, 1895) deserves special mention because the crystals of melanotekite from this locality are exceptionally sharp. One sample, USNM B15287 of the Smithsonian Institution, was provided by P. J. Dunn, who also confirmed by electron probe analysis the end-member formula $Pb_2^{2+}Fe_2^{3+}Si_2O_9$ for the Hillsboro melanotekite.

The chemical crystallographic study of kentrolite-melanotekite turned out to be a miserable problem. We spec-

0003–004X/91/0708–1389$02.00

TABLE 1. Chemical analysis of kentrolite

	A	B
PbO	59.59	61.62
ZnO	0.05	—
MgO	0.05	—
Fe_2O_3	6.62	—
Mn_2O_3	13.55	21.79
Al_2O_3	0.30	—
TiO_2	0.38	—
SiO_2	16.45	16.59
Total	96.99	100.00

Note: A. Cameca electron probe analysis. I.M. Steele, analyst. Galena (Pb), manganoan hortonolite (Mg,Mn,Fe), rutile (Ti), ZnO (Zn), and anorthite glass (Al,Si) were used as standards. B. Computed for $Pb_2^{2+}Mn_2^{3+}O_2Si_2O_7$.

TABLE 2. Experimental data for kentrolite

	Crystal-cell data
a (Å)	6.961(2)
b (Å)	11.018(3)
c (Å)	9.964(5)
V (Å^3)	764.2(2)
Space group	*Pbcn*, orthorhombic
Z	4
Formula	$Pb_2(Mn_{0.68}Fe_{0.32})_2^{3+}O_2(Si_2O_7)$
D(cal) (g·cm^{-3})	6.26
D(obs)	6.19 (Damour and vom Rath, 1881)
μ_l (cm^{-1})	473.5
$\mu_l R$	8.29
	Intensity measurements
Crystal size	sphere, $R = 87.5$ μm
Diffractometer	Enraf-Nonius CAD4
Monochromator	Graphite
Radiation	Mo$K\alpha_1$, $\lambda = 0.70930$ Å
Scan type	θ-2θ
2θ range	0.5–64.9°
Reflections measured	1620
Unique refl. $>2\sigma F_o$	1052
F_o used in last cycle	1031
Trans. factor range	0.88 to 7.54
	Refinement of the structure
R 0.047	1031 unique refl. $R = \Sigma(\lvert\lvert F_o\rvert - \lvert F_c\rvert\rvert)/\Sigma F_o$
0.052	1052 unique refl. $>2\sigma F_o$
0.058	1060 unique refl.

Note: Unit weights were used for all F_o.

ulate that other investigators studied the chemical crystallography and encountered the same thorny problems we did. The sample used by us for complete study was personally collected by the senior author on the dumps at Långban, an occurrence where members of the series were at one time quite abundant. Magnusson (1930), in his now-classic treatise on the Fe-Mn-oxide ore deposit, reported that at least one ton of melanotekite was removed from the Norrbotten stope. Over a decade ago, single crystal studies on Långban samples immediately presented problems to us. Although location of Pb^{2+} and partial structure solution was straightforward, refinements never converged below $R \sim 0.17$. Three crystals were studied and their structures refined: the Långban sample, the Chilean kentrolite (USNM R3837), and the Hillsboro melanotekite (USNM B15287). Convergences did not decrease below $R \sim 0.14$, and a consistently heavy residue (called X) remained in difference syntheses of all three studies, approximately 0.6 Å from the Pb centroid. An electron probe analysis of all three samples for Pb content gave PbO 59–63 wt% and absence of Ba. Because the PbO range includes PbO = 61.62 wt% for $Pb_2Mn_2^{3+}Si_2O_9$, we had to look elsewhere for the source of the residue X. Space groups chosen for the battery of refinements included *Pbcn* and its immediate subgroups *Pb2n*, $P2_1cn$, $Pbc2_1$, and $P2_122_1$. With the heavy metal alone, R ranged from 0.30 to 0.34 in all these determinations.

Other crystallochemical studies have been carried out. Ito and Frondel (1968) synthesized not only melanotekite but also Sc and Ga analogues. Glasser (1967) explored the melanotekite problem even further and encountered the problems that also plagued the present study, i.e., the appearance of systematically weak reflections. In particular, he challenged Gabrielson's (1962) end-centered space group $C222_1$ (orientation of our study) and with it his structure determination. Glasser mentioned that a structure redetermination was in progress, but evidently it has not materialized.

Chastened by the crystallochemical difficulties encountered by us and other researchers, we garnered material from the Långban sample, prepared a polished section for analysis with a Cameca electron microprobe, and ground a small sphere for crystal structure analysis.

EXPERIMENTAL DETAILS

Chemical composition

Analysis using the Cameca electron microprobe on three grains of Långban kentrolite-melanotekite afforded the oxide weight percentages in Table 1. On the basis of $\Sigma O^{2-} = 9$, the analysis normalizes to $Pb_{1.98}^{2+}(Mn_{1.28}^{3+}Fe_{0.61}^{3+}Al_{0.04}^{3+}Ti_{0.04}^{4+}Mg_{0.01}^{2+}Zn_{0.00}^{2+})_{\Sigma=1.98}Si_{2.02}O_{9.00}$. The major element composition is $Pb_2^{2+}(Mn_{0.68}^{3+}Fe_{0.32}^{3+})_2Si_2O_9$, a ferrian kentrolite. The minor Mg, Al, Ti, and Zn are characteristic elements in the early skarn paragenesis at Långban.

Preliminary observations on single crystal photographs

Single crystal photographs of kentrolite-melanotekite from Långban, Chile, and New Mexico were obtained from Buerger precession and Weissenberg cameras utilizing Mo$K\alpha$ radiation. We employed the same orientation throughout this study, corresponding to holosymmetric space group *Pbcn*, $a \sim 7.0$, $b \sim 11.0$, $c \sim 10.0$ Å.

The precession photographs are especially instructive. Reflections with $(h0l)$, $l = 2n$ are sharp; however, for $h = 2n$, maxima centered at $l = 2n + 1$ occur as diffuse streaks $\parallel c^*$. Reflections with $h = 2n + 1$ are extremely weak. For $(h1l)$, diffuse streaks $\parallel c^*$ occur for $h = 2n + 1$. Weak near absences occur for reflections $h = 2n$. For $(0kl)$, $k = 2n$. For $(1kl)$ diffuse streaks $\parallel c^*$ occur for $k = 2n + 1$. Weak near absences occur for reflections $k = 2n$. The observations of systematic absences are compatible with space group *Pbcn*. Space group $C2_122_1$ of Gabrielson (1962) is compatible with absence of the weak reflections. Admitting the weak reflections, Glasser's (1967) observations

are confirmed, although he did not suggest a space group. The relative intensity of streaks varies with source of the crystal, the New Mexico material showing the least streaking.

The presence of streaks indicates the presence of domains or some semirandom ordering in the structure. At best, refinement in space group *Pbcn* will provide an averaged structure. The problem is exacerbated by the presence of heavy Pb ($Z = 82$) in a relatively light matrix of other elements ($Z < 27$). We shall see that the streaks are probably caused by a split Pb centroid and that about 96% of total scattering matter is also compatible with $C2_122_1$. Finally, 34 unique nonzero reflections violate restrictions for space group *Pbcn,* but these were mostly very weak and were suppressed during refinement. It is suspected that these, too, arise from the split lead centroid.

Data measurement

Table 2 outlines the experimental details of the single crystal study. The aforementioned single crystal film results required measurement of a complete set of data including very weak reflections. The large linear atomic absorption coefficient, $\mu_l = 473.5$ cm^{-1}, necessitated use of a carefully ground sphere. We had hoped to grind single crystals of end-member compositions from Chile and New Mexico into spheres, but the members of the series are very brittle and the crystals were too small. Material from Långban proved adequate after several trials with the Bond sphere grinding method. With very slow grinding, a sphere 175 μm in diameter was obtained. The early reluctance to assume (Mn^{3+},Fe^{3+}) solid solution for a Långban crystal arose from concern that tetragonal distortion for $4d^4$ Mn^{3+} but not for isotropic $4d^5$ Fe^{3+} may add to the complex problem at hand through site splitting. This worry later proved unfounded.

Of the 1620 reflections measured to $2\theta = 65°$, 34 reflections mentioned earlier violated space group *Pbcn.* Collectively, these violations destroy all glide and screw translations found in *Pbcn* and, in conjunction with knowledge of the crystal structure, require the space group to be $P\bar{1}$. This increases the variable parameters by a factor of four. The most intense violation is $|Fo|_{100} = 114$, as compared with the strongest reflection in the data set, $|Fo|_{045} = 546$. The strongest of the violations thus yields $|Fo|^2_{100}/|Fo|^2_{045} \times 100 \sim 4\%$, demonstrating that all violations of *Pbcn* are quite weak. In fact, Glasser's (1967) (005) reflection appears among our 34 violations. Its intensity is ~1% that of (045). These violations have been listed in Table 3a.[1] They were not considered further.

Some comments on Table 2 are in order. The scan width, $\theta = (A + B \tan \theta)$ with $A = 1.10$ and $B = 0.35$, and the variable horizontal width, $W = A + B \tan \theta$ with $A = 4.0$ and $B = 1.0$, were used for the scans. The maximum scan time was 90 s, ⅙th on left and on right backgrounds and ⅔th for peak integration. Three standard reflections were monitored after every 2 h of X-ray exposure time. The orientation of three reflections was checked every 200 measurements to insure that no setting angles shifted more than 0.1°. The intensities were corrected for absorption and for Lorentz and polarization factors. The cell dimensions were obtained from least-squares fit of 25 reflections with $12° < 2\theta < 18°$. The ranges in Miller indices are $h = 0$–10, $k = 0$–16, and $l = 0$–14.

For the remaining 1052 unique reflections greater than $2\sigma F_o$, $R = 0.052$. A further problem exists with the data set that conforms to *Pbcn.* What effect does the earlier elimination of 34 weak reflections that violate *Pbcn* through a purported lone-pair effect have on the remaining 1052 reflections that conform with *Pbcn*? In the absence of criteria for suppressing such data and with reluctance to remove data arbitrarily, we suppressed 21 reflections having $||F_o| - |F_c|| > 20$. These data are listed in Table 3b. Remaining are 1031 independent reflections used in the final refinement.

At first, we tried structure refinement in space group $P\bar{1}$, but the pronounced correlations among atoms related by pseudosymmetry rendered such an approach fruitless. We feel Table 3a will prove valuable in more detailed future investigation. The appearances of weak additional intensities seem to plague data sets that involve a heavy cation with a lone pair, in this case $6s^2$ Pb^{2+}. Some other examples include dense paulmooreite, $Pb^{2+}_2As^{3+}_2O_5$ (Araki et al., 1980), and the even more exotic hyalotekite, $Pb^{2+}_2Ba_2Ca_2[(B_2Si_{1½}Be_{½})Si_8O_{28}]F$ (Moore et al., 1982). It appears that, in addition to the lone-pair effect of Pb^{2+} about its immediate neighborhood (local distortion), the effect possibly extends throughout the entire unit cell (global distortion) with disruption of symmetry.

Final refinement

A brief mention should be made of the structure solution. The broad outline of the atomic arrangement was deciphered over a decade ago by classical Patterson function, heavy atom techniques. Nine atoms in the asymmetric unit of space group *Pbcn* gave $R \sim 0.17$ and, aside from the Pb atom, bore only a feeble resemblance to the structure model proposed by Gabrielson (1962). At our early stage of study, several members of the kentrolite-melanotekite series were investigated. None afforded significant improvement, and all showed the same residue near the Pb position on the Fourier maps. The problem was therefore abandoned.

Recently, much progress has been made in the laboratory of the senior author concerning split Pb atoms. The new data set therefore was used in a refinement that included splitting of the Pb atom into xPb(1) and $(1 - x)$Pb(2) in complementary relationship to each other, in conjunction with atoms M(1), M(2), Si, and O(1)–O(5). After several cycles, R decreased to 0.08 with $x = 0.73(2)$. With the 1031 unique reflections and refinement of the anisotropic thermal vibration (displacement) parameters,

[1] A copy of Tables 3a–3c may be ordered as Document AM-91-466 from the Business Office, Mineralogical Society of America, 1130 Seventeenth Street NW, Suite 330, Washington, DC 20036, U.S.A. Please remit $5.00 in advance for the microfiche.

TABLE 4A. Kentrolite atomic coordinate parameters

Atom	P	R	x	y	z	B_{eq}
Pb(1)	0.73(2)	8	0.4561(7)	0.3012(1)	0.5500(1)	0.93
Pb(2)	0.27(2)		0.5351(22)	0.3098(3)	0.5475(2)	1.07
M(1)	1.00	4	½	0	0	0.58
M(2)	1.00	4	½	0.1482(2)	¼	0.57
Si	1.00	8	0.2140(4)	−0.0907(3)	0.2528(4)	0.50
O(1)	1.00	8	0.3402(12)	0.0054(8)	0.3361(8)	0.74
O(2)	1.00	8	0.2995(15)	−0.1135(8)	0.1031(9)	1.11
O(3)	1.00	8	0.1888(13)	−0.2217(8)	0.3272(9)	0.91
O(4)	1.00	4	0	−0.0286(13)	¼	1.88
O(5)	1.00	8	0.6094(13)	0.1442(7)	0.4227(8)	0.63

Note: Atom label, site population (P), equipoint rank number (R), atomic coordinates (*x,y,z*), and equivalent isotropic thermal parameters (B_{eq}, see Table 4b) are listed. Standard errors in parentheses refer to the last digit.

R decreased to 0.047 for 81 variable parameters, giving a data : variable parameter ratio of 12.7:1. Neutral atom scattering factors and real and imaginary dispersion corrections were taken from Ibers and Hamilton (1974). Table 3c lists the observed and calculated structure factors for the final refinement. Table 4a presents the atomic coordinate and equivalent isotropic thermal vibration parameters, and Table 4b gives the thermal vibration parameters. Note that only O(1) is weakly nonpositive definite. Table 5 provides the principal interatomic distances and angles, with emphasis placed on Pb(1) and Pb(2).

Of the ten unique atoms, only O(1), O(2), O(3), and O(5) are incompatible with space group $C222_1$ ($\equiv C2_122_1$), and this doubtless explains the *C*-centered subsymmetry and confusion in the past. Adopting general equipoints, Pb(1) = Pb(2) with coordinates ½, ¼, ½ and Si is at *xy*¼. These approximate compatible positions in space groups $C222_1$ and *Cmcm*. In fact, if the sum of the squares of the atomic numbers in the unit cell is divided into the sum of squares for atoms compatible with *Pbcn* and $C222_1$, 96.7% of the scattering matter is accounted for. Clearly, space group theory plays a big role in kentrolite-melanotekite chemical crystallographic relations.

KENTROLITE: CHEMICAL CRYSTALLOGRAPHIC RELATIONS

Kentrolite possesses an elegant structure. Although it defines a unique structure type, its fundamental building block (fbb) occurs in other structure types. In addition, earlier discussion of intensities implied a structural hierarchy that is best understood through group-subgroup relations.

Group-subgroup relations

Another phase that is closely related to kentrolite-melanotekite, synthetic CMS-X1, was investigated by Moore and Araki (1979), and good convergence was achieved ($R = 0.038$). Comparison with cell parameters and contents reported for kentrolite-melanotekite is in order and appears (rounded to the second digit) in Table 6.

The kentrolite and CMS-X1 structure types are now known. Their relation is based on the $^1_\infty M^{3+}\phi_4$ fundamental building block of edge-sharing octahedra in $\cdots cis\text{—}trans \cdots$ sequence with respect to successive adjacent octahedra. This octahedral chain is parallel to [001], the one direction nearly common to these two structure types. The chain component is now oriented in the {100} plane. Elements of symmetry can be immediately extracted: inversion at the origin, twofold rotor at (0*y*¼), and *c* glide at (*x*0*z*). The projection along [100] leads to plane group {*p*2*gm*}, the basis of the two-sided plane group (a space group) {*P*12/*c*1}. Does *P*2/*c* (projected along [100]), occur among the two structure types? Can Gabrielson's space group be related?

Define the collection of space group symmetry elements modulo the translation group T as { }. The elements in the kentrolite group are most conveniently expressed in full notation $\{P2_1/b,2/c,2_1/n\}$. The order (#) mod T or number of elements in the group is expressed by $n = |\#|$. In a group multiplication table, the order would correspond to the number of rows (or columns) of *n* elements. For $\{P12/c1\}$, $n = |4|$; $\{P2_1/b,2/c,2_1/n\}$, $n = |8|$; $\{C222_1 \equiv C2_122_1 \equiv C2_12_12_1\}$, $n = |8|$; and $\{I2/c \equiv I2_1/a\}$, $n = |8|$. Listing the equivalent set of points for each group admits those elements that are equal among the groups, either according to the representation of points or representation of elements of symmetry. This is expressed by the intersection ($\cap$) of the groups treated as sets.

The following intersections are of interest:

$$\{P2_1/b,2/c,2_1/n\} \cap \{I1,2/c1\} = \{P12/c1\}, \quad n = |4| \qquad (1)$$

TABLE 4B. Kentrolite: anisotropic thermal-vibration parameters ($\times 10^4$)

	U_{11}	U_{22}	U_{33}	U_{23}	U_{13}	U_{12}	
Pb(1)	167(13)	91(3)	96(3)	−16(3)	−11(4)	3(4)	
Pb(2)	267(45)	75(8)	64(7)	−4(6)	15(11)	39(13)	
M(1)	99(9)	60(9)	62(8)	−17(7)	−15(9)	9(9)	
M(2)	83(9)	80(9)	54(9)	0	−11(8)	0	
Si	78(13)	46(10)	66(11)	5(12)	−9(11)	13(10)	
O(1)	116(35)	72(33)	94(35)	−57(31)	−13(29)	−79(30)	NPD
O(2)	251(49)	83(37)	87(36)	−75(32)	34(34)	−54(35)	
O(3)	126(38)	125(39)	94(34)	40(31)	−11(30)	−51(32)	
O(4)	59(51)	109(57)	546(100)	0	1(66)	0	
O(5)	167(40)	34(33)	39(32)	1(25)	−18(28)	−10(29)	

Note: The U_{ij} values are coefficients in the expression $\exp[-\Sigma_{ij} U_{ij}h_ih_j]$. Estimated standard errors refer to the last digit. NPD is a weakly nonpositive-definite solution.

TABLE 5. Kentrolite polyhedral interatomic distances (Å) and angles (°)

M(1)			M(2)		
2 M(1)$^{(2)}$-O(5)$^{(2)}$	1.923(8)		2 M(2)-O(5)	1.882(8)	
2 M(1)-O(1)$^{(2)}$	1.977(8)		2 M(2)-O(3)$^{(5)}$	2.091(9)	
2 M(1)-O(2)	2.137(10)		2 M(2)-O(1)	2.108(9)	
average	2.012 Å		average	2.027	
		angle (°)			angle (°)
2 O(1)$^{(2)}$-O(5)$^{(2)}$	2.568(12)*	82.3(3)	2 O(1)-O(5)	2.568(12)*	79.9(3)
2 O(2)-O(5)$^{(3)}$	2.829(13)	88.1(3)	2 O(3)$^{(5)}$-O(5)	2.719(12)	86.2(3)
2 O(1)$^{(2)}$-O(2)	2.894(13)	89.3(3)	1 O(1)-O(1)$^{(2)}$	2.809(12)	83.5(3)
2 O(1)$^{(3)}$-O(2)	2.929(12)	90.7(3)	2 O(3)$^{(7)}$-O(5)	2.986(12)	95.6(3)
2 O(1)$^{(2)}$-O(5)$^{(3)}$	2.937(12)	97.7(3)	2 O(1)-O(3)$^{(5)}$	3.014(13)	91.7(3)
2 O(2)-O(5)$^{(2)}$	2.991(12)	91.8(3)	2 O(1)$^{(2)}$-O(5)	3.018(12)	98.1(3)
average	2.858	90.0	1 O(3)$^{(5)}$-O(3)$^{(7)}$	3.045(13)	93.4(4)
			average	2.872	90.0
Si			Pb		
				Pb(1)-X	Pb(2)-X
1 Si-O(1)	1.607(9)		1 Pb-Pb(2)	0.558(16)	—
1 Si-O(2)	1.626(10)		1 Pb-Pb(2)$^{(4)}$	3.321(14)	—
1 Si-O(3)	1.632(10)		1 Pb-M(1)$^{(2)}$	3.370(2)	3.455(4)
1 Si-O(4)	1.639(6)		1 Pb-Si(1)	3.404(4)	3.582(9)
average	1.626		1 Pb-Pb(1)$^{(4)}$	3.792(6)	3.840(20)
		angle (°)			
1 O(1)-O(4)	2.546(9)	103.3(5)		Pb(1)-O	Pb(2)-O
1 O(3)-O(4)	2.616(14)	106.2(5)	1 Pb-O(5)	2.396(8)	2.269(9)
1 O(2)-O(3)	2.646(13)	108.6(5)	1 Pb-O(2)$^{(3)}$	2.398(10)	2.521(15)
1 O(1)-O(2)	2.680(12)	112.0(5)	1 Pb-O(3)$^{(5)}$	2.452(9)	2.489(15)
1 O(2)-O(4)	2.713(11)	112.4(4)	1 Pb-O(5)$^{(4)}$	2.502(10)	3.021(18)
1 O(1)-O(3)	2.717(13)	114.1(5)	1 Pb-O(3)$^{(1)}$	2.894(10)	2.715(13)
average	2.653	109.4	1 Pb-O(2)$^{(7)}$	2.988(11)	2.771(14)
			average	2.605	2.631 Å
			[Pb-O(1)$^{(4)}$	3.602(9)	3.162(14)]

Note: Equivalent points are referred to Table 4a and appear as superscripts: (1) $-x, -y, -z$; (2) $-x, y, ½ - z$; (3) $x, -y, ½ + z$; (4) $½ + x, ½ - y, -z$; (5) $½ - x, ½ + y, z$; (6) $½ - x, ½ - y, ½ + z$; (7) $½ + x, ½ + y, ½ - z$.
* Shared edge between M(1) and M(2) polyhedra.

$$\{P2_1/b,2/c,2_1/n\} \cap \{C2_122_1\} = \{P2_122_1\}, \qquad n = |4| \quad (2)$$

$$\{P12/c1\} \cap \{P2_122_1\} = \{P121\}, \qquad n = |2|. \quad (3)$$

This immediately answers two questions. First, the kentrolite and CMS-X1 structure types share the same subgroup of order 4, namely $\{P12/c1\}$. This same group shared by the two structure types was earlier found for the $\cdots$ *cis–trans* $\cdots$ edge-sharing octahedral chain. Second, the $\{C2_122_1\}$ representation of kentrolite by Gabrielson does not include the $\{P12/c1\}$ subgroup but only half of it, namely those elements in $\{P121\}$, $n = |2|$. Lifting of the $\{C2_122_1\}$ group by taking the Cartesian product $(\cdot)$ with inversion $(\bar{1})$ leads to an orthorhombic centrosymmetric group, viz.

$$\{C222_1\}\cdot\{\bar{1}\} = \{C2/m2/c2_1/m\} \qquad |8|\cdot|2| = |16|.$$

This supergroup, *Cmcm*, is compatible with the orthohexagonal cell of $P6_3/mmc$, the group found in ideal hexagonal close packing and in many intermetallic phases.

Cation relation to URe_2

A remarkable near-isopunctal relationship exists between kentrolite (*Pbcn*) and the intermetallic low-URe_2 (*Cmcm*) structure types. Only one phase with the low-URe_2 structure type is tabulated in Villars and Calvert (1985). Hatt (1961) approximately defined both the low- and high-temperature structures for URe_2. The low-tem-

TABLE 6. Comparative data for kentrolite-melanotekite and CMS-X1

Compound	Formula	Z	a (Å)	b (Å)	c (Å)	Space group	Reference
Kentrolite	$Pb_2(Mn,Fe)_2^{3+}O_2(Si_2O_7)$	4	6.96	11.02	9.96	*Pbcn*	This study
Kentrolite	$Pb_2(Mn,Fe)_2^{3+}O_2(Si_2O_7)$	4	6.99	11.06	10.00	$C222_1$	Gabrielson (1962)
Kentrolite	$Pb_2(Mn,Fe)_2^{3+}O_2(Si_2O_7)$	4	7.00	11.04	9.97	*P****	Glasser (1967), NMNH C3223
CMS-X1	$Ca_3Mn_2^{3+}O_2(Si_4O_{12})$	4	14.26	7.62	10.02	*I*2/*c*	Moore and Araki (1979)
			$\beta = 93.27°$				

Note: The first kentrolite has $(Mn_{0.68}Fe_{0.32})^{3+}$. The transition metal contents are uncertain in the other kentrolites. The CMS-X1 is synthetic material.

TABLE 7. Comparison of atom positions of kentrolite and URe_2

Atom	x	y	z	Δ (Å)
Pb(1)	0.456	0.301	0.550	0.48
U	0.500	0.333	0.562	
Pb(2)	0.535	0.310	0.547	0.38
U	0.500	0.333	0.562	
M(1)	0.500	0	0	0.00
Re(1)	0.500	0	0	
M(2)	0.500	0.148	¼	0.21
Re(2)	0.500	0.167	¼	
Si	0.214	0.909	0.253	0.27
Re(3)	0.250	0.917	0.250	
			Mean	0.27 Å
			Range	0.00–0.48 Å

Note: Kentrolite and URe_2 coordinates rounded off to three figures. Hatt (1961) estimated ±0.01 as errors for variable coordinate parameters. Differences, Δ, based on kentrolite cell.

perature polymorph is stable below 180 °C, is orthorhombic, space group *Cmcm,* and has cell parameters $a = 5.56$, $b = 9.18$, $c = 8.51$ Å at 151 °C, $8URe_2$. Note $a:b:c = 0.606:1:0.927$, compared with $a:b:c = 0.632:1:0.904$ for our kentrolite. Both cells contain 24 atoms (cations). Above 180 °C, Hatt found a dilated version of the orthorhombic cell, that of "the C14 hexagonal Laves phase" $P6_3/mmc$, $a = 5.43$, $a\sqrt{3} = 9.41$, $c = 8.56$ Å at 213 °C, $4URe_2$, $a: a\sqrt{3}:c = 0.577:1:0.910$. Note that the axial ratios of orthorhombic and hexagonal polymorphs suggest a dilation, which is volumetrically ca. +0.8%, that is, not uniform.

Table 7 compares all unique cation positions in kentrolite with all comparable metal positions in URe_2. The difference, Δ (Å), is obtained by calculating the displacements between centroids for the two structures, scaled according to the larger kentrolite cell. For five unique cations (atoms), the mean Δ = 0.27 Å with a range 0.00–0.48 Å. This is a rather tight fit.

The relationship $4Pb_2MnMnSi_2(O_9)$-$4U_2Re(1)Re(2)$-$Re(3)_2$ was a serendipitous find. It was discovered in Villars and Calvert (1985) by examining data for orthorhombic phases with 24 atoms in the cell. That low-$8URe_2$ stands alone as a structure type is intriguing. Note that {*Pbcn*} is a subgroup of {*Cmcm*}. This and many other new oxysalt-intermetallic relations, many entirely unsuspected, have been found in the laboratory of the senior author. The recent question that looms concerns oxysalt phases that don't seem to have intermetallic counterparts. Are these oxysalt phases a part of some polysomatic series? Or have the intermetallic counterparts yet to be found? Typical of so many relationships of this sort among the more exotic structures, the structure type of the oxysalt does not display principles of anion close packing, the structure type of the intermetallic does not, or both do not.

DESCRIPTION OF THE STRUCTURE

The $^1_\infty[M^{3+}\phi_4]$ alternate *cis-trans* edge-sharing chain was discussed earlier. The chain runs parallel to [001] and is of the same type as found in CMS-X1. It is decorated on both sides by $[Si_2O_7]$ groups that share corners with it and by the disordered Pb atoms in PbO_{6+6} coordination. The best projection is along [100], shown in Figure 1. There is a suggestion of distorted hexagonal closest packing in this direction, but the distortion is considerable. The top faces of the octahedral chains are approximately parallel to {100}, and the tetrahedra have bases that are likewise approximately parallel to {100}. The silicate tetrahedra actually form oligosilicate dimers $[Si_2O_7]$, and a line piercing these pairs through Si-O-Si is parallel to the *a* axis.

This arrangement is reminiscent of the structure principals of the "second chapter" on silicates of Belov (1963). A large number of structure types from nepheline syenites involve large cations (alkalies, alkaline earths, lanthanides), smaller octahedrally coordinated cations (Mn^{2+}, Fe^{3+},Ti^{4+},Nb^{5+}), (F,OH) anions, and diortho groups or the oligosilicate dimers $[Si_2O_7]$. A relation exists between the oxyborates $[B_2O_6\square]O_2$ and oligosilicates $[Si_2O_7]F_2$, in that the translations normal to these groups are $2 \times 3.0 = 6.0$ Å and 7.0–7.4 Å, respectively. Note the vacancy □ in the oxyborates, which reduces the anionic groups to two parallel triangles. The octahedral portions of these structures correspond to the wallpaper structures of Moore and Araki (1974). In all these structures, the piercing lines through $[BO_3]$ triangular bases or $[O_3SiOSiO_3]$ dimers are parallel to lines that pierce octahedral edges. Such wallpapers conveniently exploit the (3^6) net. In kentrolite, the piercing line penetrates octahedral faces instead of edges. Furthermore, Figure 1 suggests a packing along **a** based on the (6^3) or hexagonal net. This projection can be idealized, based on such a net as shown in Figure 2. Here, the Pb, M(1), M(2), and Si cations and O(4) anion reside in the centers of hexagons, whereas O(1), O(2), O(3), and O(5) make up the nodal points of the net. Define the edge of the octahedron as *l*. To approximately evaluate *l*, all O-O′ edges associated with $2SiO_4$, $M(1)O_6$, and $M(2)O_6$ in Table 5 were averaged, giving $l = 2.759$ Å. Computing *a*, *b*, and *c* from this value and putting the experimentally determined cell edges in parentheses, we get $a' = (2\sqrt{2}/\sqrt{3})l = 4.50(6.96)$, $b' = 4l = 11.04(11.02)$, $c' = 2\sqrt{3}l = 9.56(9.96)$ Å. Relative to the determined cell edges, *b′* is increased 0.1% and *c′* is decreased 4%, but *a′* is decreased by 35% in length. Thus, in the crystal, the *a* axis is considerably expanded with respect to the ideal closest-packed model. In addition, the structure is expanded. The packing efficiency, $V_E(O^{2-}) = 21.2$ Å^3 for O in the cell and $V_E(O^{2-} + Pb^{2+}) = 17.4$ Å^3 for O plus Pb in the cell. This contrasts with magnetoplumbite, $Pb^{2+}Fe^{3+}_{12}O_{19}$, which is based on closest packing of O atoms and of Pb: $V_E(O^{2-}) = 18.1$ Å^3 and $V_E(O^{2-} + Pb^{2+}) = 17.2$ Å^3. Although the O plus Pb values match fairly well in both compounds, O packing alone is more open in kentrolite. The Pb is situated near the 2_1 screw axes that penetrate the centers of hexagons. The combination of Pb near 2_1 screw axes parallel to [100] and $[Si_2O_7]$ dimers along that direction is the reason for 35% elongation along *a* with respect to the computed model for ideal packing above.

But what is the basis for the URe_2 structure that is compared with kentrolite's cations? Its high-temperature

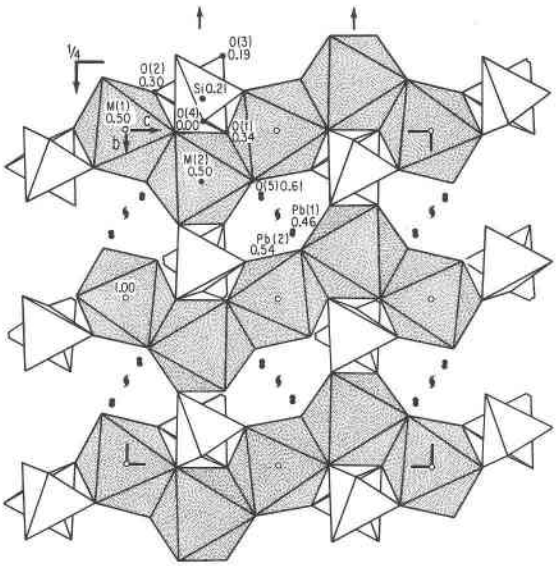

Fig. 1. Polyhedral representation of the kentrolite crystal structure projected along [100]. The Pb centroids are small circles. Heights are in fractional coordinates (x). Some symmetry elements are drawn in.

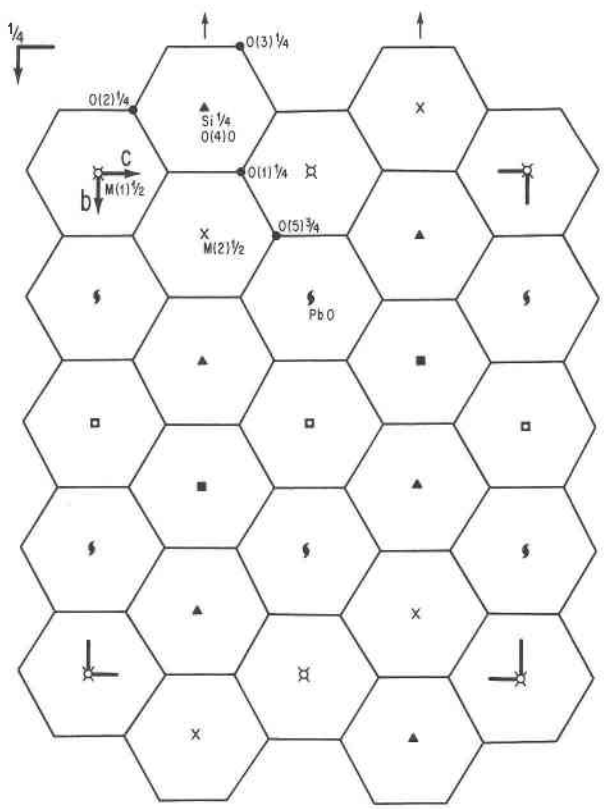

Fig. 2. The kentrolite structure as an idealized hexagonal net. Atoms in the asymmetric unit are labeled. Heights are in fractional coordinates, x. Crosses are M at x = ½, squares are M at x = 0, and triangles are Si at x = ¼ and ¾. This net is used for calculations in the text.

form (>180 °C) is a more symmetrical dilation (ΔV = +0.8%) of the orthorhombic structure, according to Hatt (1961). Using the approximate coordinates of both forms, sketches of the URe_2 "Laves phases" were made, and indeed they are closely related. Since $4URe_2$ is the cell contents for the high-temperature form with space group $P6_3/mmc$, atomic sites 2Re(1) 000; 6Re(2) 0.833, 0.660, ¼; 4 U ⅓, ⅔, 0.062 (ca. 1/16); and lattice parameters a = 5.43, c = 8.56 Å, it is more convenient to discuss this form. In addition, it has the $MgZn_2$ structure type that includes over 390 phases according to Villars and Calvert (1985). The structure is interesting enough to warrant a drawing in Figure 3.

The Re(2) comprises two (6·3·6·3) Kagomé nets that are related by inversion in the cell. As a Kagomé net is a portion of the closest-packed (3^6) planar net with three out of four sites occupied in an ordered fashion, the layers in the cell can be written 6Re(2) + 2□(2), □ denoting ordered vacancy. We label the net at z = ¼ by B and that at z = ¾ by C. The 2Re(1) are situated at 000 and 0,0,½; call this layer A. Six ordered vacancies occur, 6□(1), at (½,0,0) etc. Thus, only two out of eight sites are populated. Finally, the 2□ at (⅓, ⅔, ¼) and (⅔, ⅓, ¾) are replaced by 4U at z ca. 1/16, 7/16; 9/16, 15/16. Simple transformation to the orthohexagonal cell yields high URe_2 → kentrolite: 4Re(1) → 4M(1), 12Re(2) → 4M(2) + 8Si, and 8U → 8Pb. Counting only $[Re(1)_2\square(1)_6][Re(2)_6\square(2)_2]$, the framework of the structure is based on the sequence ·ABAC· ≡ ·ch· or double hexagonal closest packing. This can be seen in Figure 3. The same cation packing was found for the intriguing phase occurring in a similar paragenesis, långbanite.

One wonders if a high-temperature phase for the ferric analogue, melanotekite, exists that is based on the high-URe_2 ($MgZn_2$) structure. It would have space group $P6_3/mmc$ and clearly would involve some rearrangement of the oxide Lewis octets to satisfy the requirements of this group.

Bond Valences

The kentrolite crystal structure presents a peculiar problem in chemical crystallographic relations: not one but two distinct ionic species necessarily force local polyhedral distortions in the structure for two related but distinct reasons. These ions are $4d^4$ Mn^{3+} and $6s^2$ Pb^{2+}. Both ions force polyhedral distortions arising from electron-electron repulsions. The $4d^4$ Mn^{3+} ion possesses four valence electrons in high-spin arrangement induced by the surrounding oxide ligands. Three electrons of like spin populate the t_{2g} suborbitals whose three lobes are tucked between the Cartesian axes of the coordinating octahedron. The remaining fourth electron, also of like spin, populates the e_g level, which is split into an equatorial $d_{x^2-y^2}$ lobe and an apical d_{z^2} lobe. The two e_g lobes are directed along the axes of the coordinating octahedron, and electron populations in these lobes experience a pronounced repulsion from their nearest ligands. Thus, an electron in $d_{x^2-y^2}$ (along

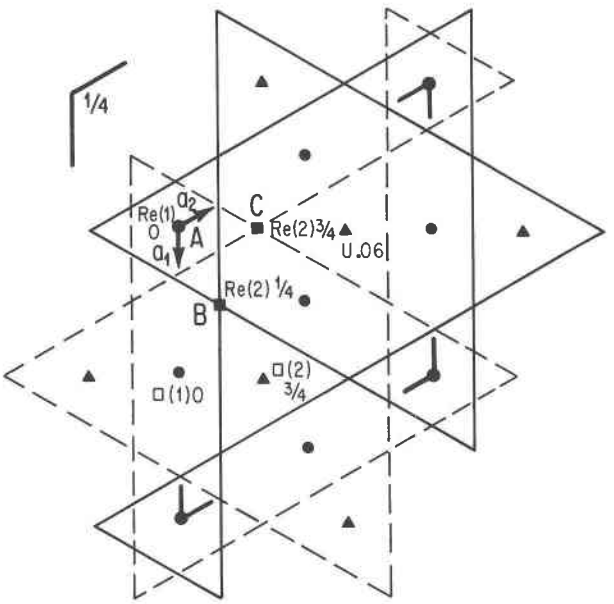

Fig. 3. Representation of the hexagonal URe_2 Laves phase, which is compared in the text with cations of the kentrolite structure. Heights in z and one mirror plane in $P6_3/mmc$ are shown. Vacancies □(1) at ½,0,0, etc. and □(2) at ⅔,⅓,¾, etc. are situated at dots (inversion centers) and triangles (threefold axes), respectively. The Kagomé net [Re(2) at square nodes] at z = ¼ is bold; its inverse at z = ¾ is dashed. The U atoms are on threefold axes at ⅓, ⅔, z, etc., and Re(1) is at the origin, etc.

x and y axes of coordinating ligands) will result in an equatorial expansion that creates a compressed octahedron or oblate spheroid. If the electron populates d_{z^2} (along the z axis of coordinating ligands), an elongate octahedron results, or a prolate spheroid. These repulsions constitute the familiar Jahn-Teller distortions away from the regular octahedron. See Burns (1970) for a concise and accurate description of the effect. The $6s^2$ Pb^{2+} ion is related in also involving electron repulsions from the coordinating ligands, but the cause arises from a centroid of lone-pair electrons interacting with adjacent bond pairs between cation and ligands; see Gillespie (1972) for a description of this effect. Both cases—Jahn-Teller and lone-pair—create distortions. Can these distortions be used to put reins on bond distance ranges in coordination polyhedra? We submit a simple, qualitative approach. We caution that ions in crystals, unlike free ions, are subject to many forces influenced by their often complex and unsymmetrical neighborhoods, so any model can only be approximate.

Pauling (1929) proposed the simple yet conditionally effective electrostatic valence rules. The rules are conditional because they apply only to spherically symmetric ions, e.g., cations stripped of their valence electrons and anions that are quite electronegative and therefore form closed Lewis octets. These rules are usually wanting for nonspherical ions discussed above. They work, however, for structures where pronounced cation-cation repulsions occur between such spherical ions. Brown (1981), in a culmination of a series of studies, presented the bond-valence method. Bond valence is much like Pauling's bond strength, as individual bonds are involved. Both are expressed as s (in electrostatic units). The principal difference is that the Brown model proceeds with an inverse power or logarithmic function with two fitted constants, and the individual bond distance is inserted. From this, bond valence is computed. For bond distances calculated from radii of Shannon and Prewitt (1969), the computed bond valence is near Pauling's bond strength. However, a Brown bond valence sum about an anion can deviate considerably from expected anion charge where pronounced cation-cation repulsion effects occur, invariably exhibiting substantial underbonding by cations. For this reason, both the Pauling and the Brown methods are adequate in most cases but remain flawed in certain cases, such as nonspherical ions and cation-cation repulsions, respectively.

We propose to compare three approaches: Pauling, Brown, and this study. The results appear in Table 8. Our approach proceeds in the same fashion as that of Kampf and Moore (1976) and Moore et al. (1991) and arose from the need to accommodate nonspherical ions into the Pauling model. In these cases involving $Mn^{3+}O_6$, deviations of up to ±0.50 esu, a considerable difference, were encountered for the simple spherical model. The model assumes spheres for ions with no valence electrons, and distortions of spheres of oblate (compressed) or prolate (elongated) spheroids for the Jahn-Teller distorted polyhedron of anions about a cation. Both are uniaxial ellipsoids. We did not consider the general case of the ellipsoid with two axes of revolution about circular sections. "Jahn-Teller tetragonal distortion" (uniaxial ellipsoid) is a common term, a consequence either of $d_{x^2-y^2}$ or of d_{z^2} electron populations. For all t_{2g} and e_g suborbitals populated in high spin arrangements such as $4d^5$ Mn^{2+}, a uniform isotropic expansion is expected and was found in the many examples of $^{[6]}Mn^{2+}$-O average distances of 2.22 Å. Notice that when all spins are paired as in $4d^{10}$ Zn^{2+}, the distance average is contrated, e.g., $^{[6]}Zn^{2+}$-O = 2.14 Å. Whether $d_{x^2-y^2}$ (oblate) or d_{z^2} (prolate) is at lower energy usually cannot be predicted without structural information.

Our crystal has sites populated approximately with $(Mn_{2/3}, Fe_{1/3})^{3+}$, and the Jahn-Teller effect should thus be apparent ($4d^5$ Fe^{3+} in high spin will be spherical). In our Table 5 of bond distances, M(1) and M(2) each have paired distances imposed by symmetry: M(1)-O(5) 1.92 (×2), M(1)-O(1) 1.98 (×2), M(1)-O(2) 2.14 (×2); M(2)-O(5) 1.88 (×2), M(2)-O(3) 2.09 (×2), M(2)-O(1) 2.11 (×2) Å. Averaging, we get M(1)-O 1.95 (×4) and 2.14 (×2); and M(2)-O 1.88 (×2) and 2.10 (×4). Note that short M(2)-O(5) are in *trans* position in the polyhedron. The short bond distances are apportioned to t_{2g} and the long repelling distances to e_g. Averaging appears reasonable (<0.03 Å difference from crystal refinement), bearing in mind that other electrostatic distortions also contribute. The $M(1)O_6$ polyhedron approximates a prolate spheroid (d_{z^2}) and the

TABLE 8. Kentrolite bond valences

	O(1)	O(2)	O(3)	O(4)	O(5)	
						Cation sum→
M(1)	× 2	× 2			× 2	
	0.543→	0.354→			0.632→	
	× 1↓	× 1↓			× 1↓	3.06
M(2)	× 2		× 2		× 2	
	0.382→		0.398→		0.711→	
	× 1↓		× 1↓		× 1↓	2.98
Si	× 1	× 1	× 1	× 1		
	1.066→	1.011→	0.994→	0.975→		
	× 1↓	× 1↓	× 1↓	×2↓		4.05
Pb(1)	× 1	× 1	× 1		× 1	
	0.044→	0.415→	0.367→		0.417→	
	× 1↓	× 1↓	× 1↓		× 1↓	1.84
		× 1	× 1		× 1	
		0.124→	0.148→		0.329→	
		× 1↓	× 1↓		× 1↓	
			Anion sum [Pb(1)]			
			↓			
B	2.04	1.90	1.91	1.95	2.09	
Pb(2)	× 1	× 1	× 1		× 1	
	0.091→	0.315→	0.338→		0.564→	
	× 1↓	× 1↓	× 1↓		× 1↓	1.82
		× 1	× 1		× 1	
		0.188→	0.210→		0.117→	
		× 1↓	× 1↓		× 1↓	
			Anion sum [Pb(2)]			
			↓			
	2.08	1.87	1.94	1.95	2.02	

Note: With Brown (1981) bond valence sums as basis [B, for Pb(1)], the Pauling (1960) spherical model (P) and the ellipsoidal model of this study (M) are

P	2.00	2.17	2.17	2.00	1.67
	(−2.0)	(+14.2)	(+13.6)	(+2.5)	(−20.1)
M	2.00	2.00	2.08	2.00	1.92
	(−2.0)	(+5.3)	(+8.9)	(+2.5)	(−8.1).

The differences (%) with B as reference are listed parenthetically.

$M(2)O_6$ polyhedron corresponds to an oblate spheroid ($d_{x^2-y^2}$ electron population), the former being more frequently encountered for Mn^{3+}.

Pauling-type bond strengths were then assigned. For M(1), $s = 7/12$ for each of the four short distances and $s = 4/12$ for each of the two long distances. For M(2), $s = 8/12$ for each of the two short distances and $s = 5/12$ for each of the four long distances. These strengths were considered reasonable values for mean Mn^{3+}-O 2.02 Å ($\langle s \rangle = 6/12$) from well-refined structures. The sum about M(1) is $4(7/12) + 2(4/12) = 36/12$ and about M(2) is $2(8/12) + 4(5/12) = 36/12$, or cation charges for each equal to 3+. The Pb(1) site which occupies about ¾th of its split position is six-coordinated for Pb(1)-O < 2.99 Å but has additional six coordination for Pb-O > 3.44 Å. An argument based on the inverse square law of Coulomb force would suggest contribution by the second sphere of coordination is weak, and it was disregarded. Only O(2), O(3), and O(5) coordinate in pairs to Pb(1). The averages of each of the three pairs are quite similar, and Pb(1)-O was assigned $s = 2/6$. The bond strength sums for the stipulations stated are O(1): $7/12 + 5/12 + 12/12 = 2.00$, O(2): $4/12 + 4/12 + 4/12 + 12/12 = 2.00$, O(3): $5/12 + 4/12 + 4/12 + 12/12 = 2.08$, O(4): $12/12 + 12/12 = 2.00$, and O(5): $7/12 + 8/12 + 4/12 + 4/12 = 1.92$ esu. These results, listed in Table 8, give a mean Δ magnitude of 5.4% (the Pauling spherical model gives 10.5%) when compared with the Brown bond valence sums for five independent anions.

Why is such a lengthy discussion of bond valences offered? The reason is that both the entrenched Pauling and more recently fashionable Brown models have advantages and pitfalls. We believe that our approach toward nonspherical cations (e.g., valence electrons remaining) is a better picture of reality than the Pauling spherical model. It compares reasonably well with the Brown bond valence model, which also seems to accommodate Jahn-Teller cations and lone-pair systems as well, presumably because it is a charge-conserving system based on individual bond distances to an anion. The application of the Brown model to squares of edge-sharing octahedral cations with focus on the anion in the center, however, is much less satisfying, even though the Pauling model applied to the same cluster seems to work (this will be reported in a separate note). It is concluded that the Brown model is very sensitive to cation-cation repulsion effects and, in extreme cases, is unsatisfactory.

Is the coexistence of $Mn^{3+}(1)$, point symmetry $\bar{1}$ as a prolate spheroid and $Mn^{3+}(2)$, point symmetry (2) as an oblate spheroid reasonable in the same crystal? The Jahn-Teller theorem predicts distortion but cannot predict the kind of distortion or the electron population either in $d_{x^2-y^2}$ or d_{z^2}. Recourse must be made to an independent experiment, in our case crystal structure analysis. The same ···*cis–trans*··· octahedral edge-chain was noted by Moore and Araki (1979) in well-refined ($R = 0.04$) syn-

thetic CMS-X1 or $Ca_3Mn_2^{3+}O_2(Si_4O_{12})$. Here, the same point symmetries occur about Mn(1) and Mn(2) but in reverse order. The distances 2Mn(1)-O(7) = 1.86, 2Mn(1)-O(5) = 2.07, and 2Mn(1)-O(6) = 2.16 by averaging corresponds to 2Mn(1)-O = 1.86 and 4Mn(1)-O = 2.12 Å, an oblate spheroid. It has point symmetry ($\bar{1}$) and distances similar to those for kentrolite. The distances 2Mn(2)-O(7) = 1.88, 2Mn(2)-O(4) = 1.96, and 2Mn(2)-O(5) = 2.30 Å by averaging corresponds to 4Mn(2)-O = 1.92 and 2Mn(2)-O = 2.30 Å, a prolate spheroid. The long Mn(2)-O(5) distances are in *trans* position in the polyhedron. It has point symmetry (2). Note that comparison with kentrolite must take into account that CMS-X1 is a pure Mn^{3+} salt, but kentrolite has ca. ⅓ Fe^{3+}, a spherical ion, mixed over the M sites. Although Mn^{3+} in both kentrolite and CMS-X1 comprise the same kinds of $^1_\infty MO_4$ chains, their environments are quite different. Clearly, neighborhood plays a fundamental role, but static Jahn-Teller distortion appears to prevail. Note again that the point symmetries of the prolate and oblate spheroids are reversed in one crystal with respect to the other.

In bermanite (R = 0.06, Kampf and Moore, 1976), $Mn^{2+}(H_2O)_4[Mn_2^{3+}(OH)_2(PO_4)_2]$, the two unique $Mn^{3+}\phi_6$ polyhedra possess point symmetry 1. The 1.89–1.96 Å collective range for four equatorial Mn^{3+}-ϕ distances and the range 2.20–2.24 Å for two apical distances in these two polyhedra indicate that both are prolate spheroids. The $^1_\infty Mn^{3+}\phi_4$ edge-chain is linear; that is, the $Mn^{3+}\phi_6$ are in ··*trans*·· arrangement only. Accurate crystal structure refinements of the Fe^{3+} end-members of these compounds would be informative.

Kentrolite: Pb (II) lone pairs

Only recently have heavy cations with affixed lone-pair electrons been investigated in detail for oxysalt crystals. Crystals of Tl^{1+}, Pb^{2+}, Bi^{3+}, In^{1+}, Sn^{2+}, and Sb^{3+} oxysalts characteristically possess $\mu_l > 300$ cm^{-1}, and such a high absorption coefficient hampers suitable convergence to $R < 0.04$. For this reason, small spheres are often ground so that a suitable absorption correction can be applied. Convergence at a low R factor is necessary for determination of meaningful (and reliable) interatomic distances and angles to light atoms (such as O) in the presence of heavy atoms (such as Pb).

Recently, Hyde and Andersson (1989) devoted a chapter on lone-pair electrons and presented some crystal structures in which they occur. Sidgwick and Powell (1940) assumed the electronic bond pair (bp) between two nuclei and the lone pair (lp) attached to only one nucleus were spatially arranged to minimize interelectronic repulsions. Gillespie and Nyholm (1957) assumed that the lp is spatially larger than the bp and that repulsion decreases lp − lp > lp − bp > bp − bp. Their model had ligands at corners of a polyhedron, the cation nucleus residing in the center of that polyhedron. The larger lp distorts the polyhedron because of lp − bp repulsions, and such polyhedra can be quite distorted. Such distortion is apparent in the extensive range of distances between nucleus and ligands. In other words, the ligands are forced to move off the vertices of a regular polyhedron.

Culminating a series of investigations, Hyde and Andersson (1989) proposed a regular polyhedral model where the lp and the ligands are placed at the vertices. The nucleus, however, is displaced from the center of the polyhedron toward the lp. Physically, this arises because the lp is attached to only one nucleus, so the nucleus-lp distance is relatively short (~1.0 Å) compared with the nucleus-ligand distance (~2.0 Å).

In all these studies, however, no mention is made of the direction in which the nucleus will move in a given crystal structure. We propose to wed the Hyde and Andersson (1989) model with the Pauling (1929) model of electrostatic neutrality of cations about anions. In this manner, we envision an explanation of polyhedral distortions that is ultimately based on Coulombic electrostatics. Most of this discussion of kentrolite exploits the array of bond valences and bond valence (strength) sums by three different approaches in Table 8.

The Pauling spherical model, based on cation charge and coordination number of anions about that cation, is a kind of average. Large differences of bond strength sum from anion charge magnitude should tell us something about cations that are not in fact spherical but that have some valence electrons remaining. In a sense, the simplest model seems to be the most sensitive: the Brown model, although usually affording better match of bond valence sums with ion charges, incorporates individual distances in the bond valence calculation. Some information (other than cation-cation repulsions) may be lost. In Table 8, we see that O(5) is undersaturated by −⅓ esu according to the Pauling model, the other anions being neutral or a bit oversaturated. We would immediately predict from this spherical model that, on electrostatic grounds, the Pb^{2+} cation in a polyhedron with 2O(2), 2O(3), and 2O(5) at the vertices would move toward the most undersaturated anion and that the lone pair of electrons will tend to be situated with its sphere of influence toward the more oversaturated opposing anions.

This is precisely what happens in kentrolite for both Pb(1) and its split equivalent, Pb(2); that is, Pb(1)-O(5) = 2.396 and Pb(2)-O(5) = 2.268 Å are the shortest distances found in each polyhedron. From the Pauling model, we conclude that Pb will move toward O(5), beginning with the spherical case. The Brown model (Table 8) clearly shows how O(5) is almost exactly balanced by its continguous bond valences. Both M(1) and M(2) contribute their shortest bonds to O(5). In addition, the short Pb-O(5) distances provide large bond valences to O(5). Together, the sums according to the Brown model lead to, if anything, a slight overbonding of O(5), which is distinct from the substantially undersaturated O(5) in the Pauling model.

In this and in other tested structures, the Pauling model appears to be a rather faithful means of predicting cation

movements in oxide Lewis octets and in systems involving cation lone pairs. Why Pb(1) and Pb(2) are unsymmetrically split remains an unanswered question.

As yet, no single, simple, predictive theory has evolved from the startling and unexpected intermetallic-oxysalt relationships. Perhaps through further documentation and illustration of this apparently fundamental relation, the realization of what predicates structure type itself will be revealed to us.

Acknowledgments

Aside from comments in the text, John S. White, Jr. of USNM was most helpful in the initial stage in rounding up some samples from the museum's extensive collection.

J.S. thanks the Ministry of Education, Peoples' Republic of China, for his support during studies here, P.K.S. acknowledges the Tennessee computation facilities at the Tennessee Earthquake Information Center for time on their VAX Computer, and P.B.M. appreciates NSF's forbearance toward a simple problem that became complex, through grants EAR-8408164 and EAR-8707382.

References cited

Araki, T., Moore, P.B., and Brunton, G.D. (1980) The crystal structure of paulmooreite, $Pb_2As_2O_5$: Dimeric arsenite groups. American Mineralogist, 65, 340–345.

Belov, N.V. (1963) Crystal chemistry of large cation silicates, 162 p. Consultants Bureau, New York.

Brown, I.D. (1981) The bond valence method: An empirical approach to chemical structure and bonding. In M. O'Keeffe and A. Navrotsky, Eds., Structure and bonding in crystals, vol. 2, p. 1–30. Academic Press, New York.

Burns, R.G. (1970) Mineralogical applications of crystal field theory, p. 4–127. Cambridge University Press, New York.

Damour, A., and vom Rath, G. (1881) Ueber den Kentrolith, eine neue Mineralspecies. Zeitschrift für Krystallographie, 5, 32–35.

Flink, G. (1891) Kentrolit von Långbanshyttan, Mineralogische Notizen III. Kongliga Svenska Vetenskapsakademiens Handlingar Bihang, 16, II nr. 14, 14.

Gabrielson, O. (1962) The crystal structures of kentrolite and melanotekite. Arkiv för Mineralogi och Geologi, 3, 141–151.

Gillespie, R.J. (1972) Molecular geometry. Van Nostrand–Reinhold, London.

Gillespie, R.J., and Nyholm, R.S. (1957) Inorganic stereochemistry. Quarterly Review of the London Chemical Society, 11, 339–380.

Glasser, F.P. (1967) New data on kentrolite and melanotekite: Ternary phase relations in the system PbO-Fe_2O_3-SiO_2. American Mineralogist, 52, 1085–1093.

Hatt, B.A. (1961) The crystal structure of URe_2. Acta Crystallographica, 14, 119–123.

Hyde, B.G., and Andersson, S. (1989) Inorganic crystal structures, p. 257–271. Wiley, New York.

Ibers, J.A., and Hamilton, W.C., Eds. (1974) International tables for X-ray crystallography, vol. 4, p. 99–100. Kynoch Press, Birmingham, England.

Ito, J., and Frondel, C. (1968) Syntheses of the scandium analogues of aegirine, spodumene, andradite and melanotekite. American Mineralogist, 53, 1276–1280.

Kampf, A.R., and Moore, P.B. (1976) The crystal structure of bermanite, a hydrated manganese phosphate mineral. American Mineralogist, 61, 1241–1248.

Lindström, G. (1880) Analyser av tvenne mineral från Långban. Kongliga Svenska Vetenskapsakademiens Förhandlingar Öfversikter, 35, nr. 6, 53.

Magnusson, N.H. (1930) Långbans Malmtrakt. Sveriges Geologiska Undersökning, Serie Ca, no. 23, p. 49–51, Stockholm, Kungliga Boktryckeriet.

Moore, P.B., and Araki, T. (1974) Pinakiolite, wightmanite and warwickite: Crystal chemistry of complex 3 Å wallpaper structures. American Mineralogist, 59, 985–1004.

——— (1979) Crystal structure of synthetic $Ca_3Mn_2^{3+}O_2[Si_4O_{12}]$. Zeitschrift für Kristallographie, 150, 287–297.

Moore, P.B., Araki, T., and Ghose, S. (1982) Hyalotekite, a complex lead borosilicate: Its crystal structure and the lone-pair effect of Pb(II). American Mineralogist, 67, 1012–1020.

Moore, P.B., Sen Gupta, P.K., and Le Page, Y. (1991) The remarkable långbanite structure type: Crystal structure, chemical crystallography, and relation to some other cation close-packed structures. American Mineralogist, 76, 1408–1425.

Pauling, L. (1929) The principles determining the structure of complex ionic crystals. Journal of the American Chemical Society, 51, 1010–1026.

——— (1960) The nature of the chemical bond (3rd edition), p. 543–562. Cornell University Press, Ithaca, New York.

Shannon, R.D., and Prewitt, C.T. (1969) Effective ionic radii in oxides and fluorides. Acta Crystallographica, B25, 925–945.

Sidgwick, N.V., and Powell, H.M. (1940) Stereochemical types and valency groups. Proceedings of the Royal Society of London, A176, 153–160.

Villars, P., and Calvert, L.D. (1985) Pearson's handbook of crystallographic data for intermetallic phases, vols. 1–3, 3258 p. American Society for Metals, Metals Park, Ohio.

Warren, C.H. (1895) Mineralogical notes, 1. On the occurrence of melanotekite at Hillsboro, New Mexico, and on the chemical composition of melanotekite and kentrolite. American Journal of Science, 156, 116–119.

Manuscript received September 11, 1990
Manuscript accepted April 8, 1991